Wave Statistics and Space-time Extremes via Stereo Imaging

Francesco Fedele
School of Civil and Environmental Engineering and School of Electrical and Computer Engineering
Georgia Institute of Technology, Atlanta, Georgia, USA

Alvise Benetazzo
Institute of Marine Sciences, Italian National Research Council
Venice, Italy

Guillermo Gallego
Grupo de Tratamiento de Imágenes, Universidad Politécnica de Madrid
Madrid, Spain

Ping-Chang Shih, Anthony Yezzi
School of Electrical and Computer Engineering, Georgia Institute of Technology
Atlanta, Georgia, USA

Francesco Barbariol
Department of Civil, Environmental and Architectural Engineering, University of Padua
Padua, Italy

ABSTRACT

We present an analysis of the space-time dynamics of oceanic sea states exploiting stereo imaging techniques. In particular, a novel Wave Acquisition Stereo System (*WASS*) has been developed and deployed at the oceanographic tower *Acqua Alta* in the Northern Adriatic Sea, off the Venice coast in Italy. The analysis of *WASS* video measurements yields accurate estimates of the oceanic sea state dynamics, the associated directional spectra and wave surface statistics that agree well with theoretical models. Finally, we show that a space-time extreme, defined as the expected largest surface wave height over an area, is considerably larger than the maximum crest observed in time at a point, in agreement with theoretical predictions.

KEY WORDS: Stereo measurement; *WASS*; Wavenumber-frequency spectrum; Wave statistics; Space-time extremes.

INTRODUCTION

Wave extreme predictions are typically based on the statistical analysis of time series of the wave surface displacements retrieved from wave gauges, ultrasonic instruments or buoys at a fixed point P of the ocean. However, the limited information content of point measurements does not allow accurate predictions of the space-time wave dynamics and the associated extremes. Indeed, recently some authors (Forristall, 2006; Forristall, 2007; Fedele et al., 2011; Fedele 2012) have shown that the maximum surface height over a given area of the ocean is generally larger than that observed in time via point measurements. In particular,

in short-crested seas the surface time series gathered at the given location tends to underestimate the true actual wave surface maximum that can occur over a given region of area E_s around P. The probability that the group passes at its apex through P is practically null, because large waves travel on top of wave groups. The large crest height recorded in time at P is simply due to the dynamical effects of a wave group that focuses nearby that location within or outside E_s forming a larger wave crest. Clearly, point measurements can underestimate the maximum wave group surface height attained over E_s, which is not necessarily the highest crest height of the group, unless the area is large enough to embed the entire group dynamics. Only in narrow-band sea states, point measurements are exact in predicting such maximum, which is expected to be the same at any point in space. However, realistic oceanic conditions are generally short-crested. Quantifying such underestimation is of relevant significance in offshore industry for a proper design of the air gap under the deck of fixed offshore structures. Indeed, localized damages have sometimes been observed on the lower decks of platforms after storms (Forristall, 2006; Forristall, 2007). This may occur when the design is based on the expected largest crest height from point measurements, which underestimates the expected global maximum, i.e. the largest wave surface height over the rig's area footprint. At these scales and smaller, the radar or SAR remote sensing is not accurate enough to reconstruct the space-time dynamics and associated spectral properties. A two dimensional wave probe-type array could be used, but it can be expensive to install and maintain.

Stereo video techniques can be effective for such precise measurements that are also beneficial in other applications, such as the validation of

remote sensing data and the estimation of dissipation rates and statistics of breaking waves for the correct parameterization of numerical wave models. A stereo camera view provides both spatial and temporal data whose statistical content is richer than that of a time series retrieved from wave gauges (Benetazzo, 2006; Benetazzo et al., 2012; Fedele et al., 2011; Gallego et al., 2012). In practice, since the water surface is a specular object in rapid movement, each stereo-pair is acquired simultaneously and the geometry of the stereo system is defined so to minimize errors due to sea surface specularities (Jahne, 1993). Further, the reconstruction of the water surface usually relies on epipolar techniques (Benetazzo, 2006; Benetazzo et al., 2012), which find pixel correspondences in the two synchronized images by a pixel-by-pixel-based search that is computationally expensive. Therefore, only in the last two decades or so, stereo imaging has become more suitable for applications in oceanography with the advent of high performance computer processors. For example, Shemdin et al. (1988) and Banner et al. (1989) estimated directional spectra of short gravity waves and Benetazzo (2006) and Benetazzo et al. (2012) proposed and optimized a Wave Acquisition Stereo System (*WASS*) for field measurements at the coast.

In this work, we present an application of *WASS* to investigate both space-time and spectral properties of oceanic sea states via offshore stereo measurements of gravity waves over large areas ~1100 m^2. *WASS* was deployed at the oceanographic tower *Acqua Alta* in the Northern Adriatic Sea, off the Venice coast in Italy (Cavaleri et al., 1997). Video data of sea states were acquired in three experiments carried out during the period 2009-2010 and validated against point probe measurements available at *Acqua Alta*. In particular, our analysis show that the wave statistics agree well with theoretical models and that the vertical profile of the current flow underneath the wave surface can be estimated from the wavenumber-frequency spectrum. Further, for the observed stationary sea states, we also investigate their space-time extremes, which are defined as the largest surface wave heights expected over a given area during the sea state duration (~30 min). Such extremes depend upon the directional wave spectrum of the sea state and fairly agree with the predictions based on stochastic theories for maxima of Gaussian fields (Adler, 1981; Adler, 2000; Piterbarg, 1995; Adler and Taylor, 2007).

and sea temperature. Conventional tide and wave gauges are also operational, together with a NORTEK AS AWAC Acoustic Doppler Current Profiler (ADCP) installed eastward, approximately 20 m away from the platform's legs.

WASS was installed permanently on the North-East side of the tower in order to expose the stereo field of view to Breeze and Sirocco wind conditions (blowing approximately from South-East), as well as Bora (blowing approximately from North-East). Such configuration minimizes diffraction effects due to the platform. Further, to maximize the common field of view of the two cameras, i.e. stereo pairs, *WASS* was deployed at approximately 12.5 m above the mean sea level on the third floor of the platform. In such setting, the stereo pairs cover a common trapezoidal area with sides of length 30 m and 100 m, respectively, and a width of 100 m as shown in Fig. 2. The resulting imaged area is approximately 1100 m^2. The deployed *WASS* consists of two BM-500GE JAI digital cameras (2456 x 2058 CCD active pixels with a square cell size of 3.45 μm x 3.45 μm, and a 8-bit based dynamical range) mounting 5-mm focal length low distortion lenses. The baseline between the two cameras is set at 2.5 m. Cameras are synchronized by an external trigger that allows 5,10, and 15 Hz frame acquisition rates. Synchronization delay is kept within 1 ms as required for wave measurements (Holthuijsen, 1983). For each camera, digital image data transfer rate up to 75 Megabyte/s is managed by a dedicated Giga Ethernet device and high performance Hard Drives at the acquisition workstation (Fig. 1, Right). Such stereo system must be calibrated. To do so, standard image analysis techniques (Ma et al., 2004) exploit a given known reference (for example, a chess-board) to estimate internal parameters such as lens focal length, principal point and distortion, i.e. lens angular aberration as well as external parameters, which yield the reciprocal position of the two cameras with respect to a fixed reference world system. At *Acqua Alta*, five calibration sessions were performed.
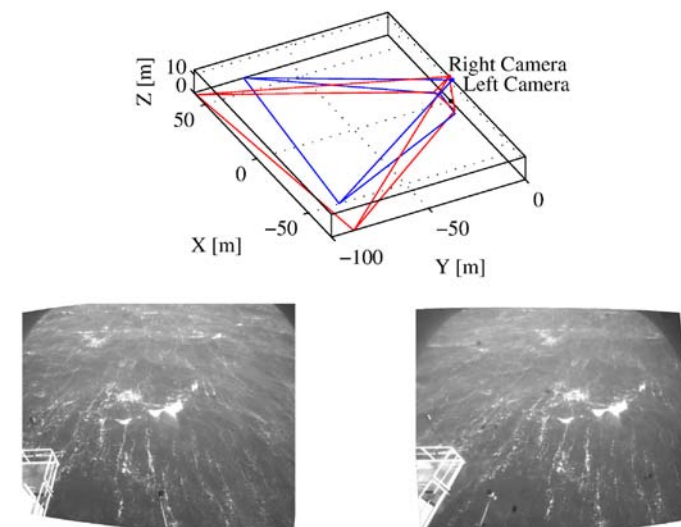

Fig. 2 - *WASS* deployment at *Acqua Alta*. Top: Left (blue lines) and Right (red lines) camera fields of view. The origin of world coordinate system (*X,Y,Z*) is on the vertical projection of the Left camera principal point on the mean water surface horizontal plane. The *Y* axis was approximately set parallel to the North-East direction. Bottom: Example of synchronized images of the sea framed by Left and Right cameras.
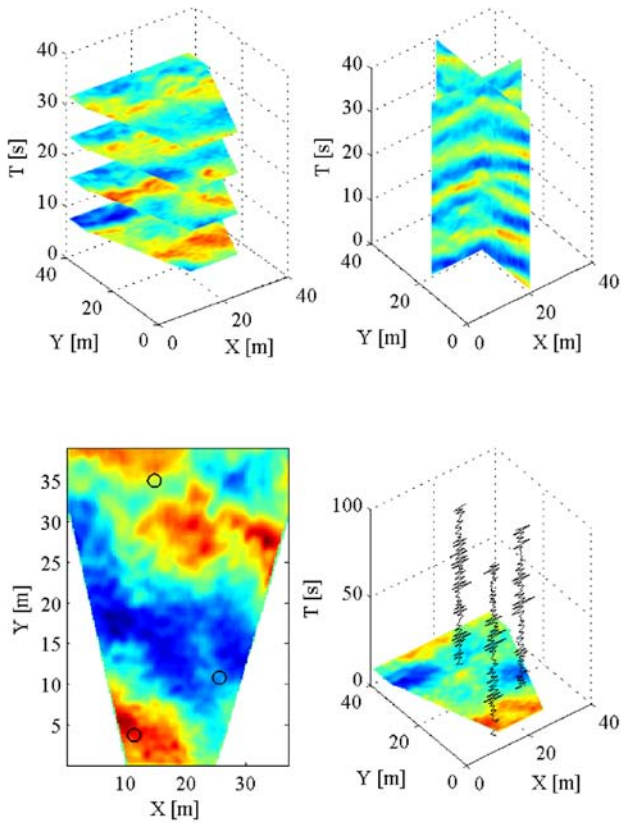

Fig. 1 - Left: CNR-ISMAR oceanographic platform *Acqua Alta* off the Venice coast in Italy. Center: deployed *WASS*. Right: *WASS* data acquisition workstation.

STEREO IMAGING

WASS Deployment at *Acqua Alta*

The oceanographic platform *Acqua Alta* (Fig. 1, Left) is located in the Northern Adriatic Sea (45° 18.83' N, 12° 30.53'E), 10 miles off the coastline of Venice, on 16 meters deep waters. The platform is managed by the Marine Science Institute of the Italian National Research Council (CNR-ISMAR). *Acqua Alta* is equipped with a meteo-oceanographic station that provides measurements of wind, temperature, humidity, solar radiation, rain, waves (directional), tides

Fig. 3 - Experiment 2: 4-D space-time wave volume *V*. Top-left: Horizontal slicing of *V* (sequence of snapshots). Top-right: Vertical slicing of V. Bottom-left: some of the virtual probes (black circles) on the *XY* plane used to validate *WASS* measurements, Bottom-right: Extracted wave time series at given virtual point probes.

Experimental campaigns

Stereo video sequences were acquired by *WASS* in three experimental campaigns at *Acqua Alta* during 2009-2010 under both Bora and Sirocco wave climate conditions, as shown in Table 1. In the same Table, for each experiment, we also report the acquisition starting date, the sequence duration, the number of acquired frames and associated rate. The three experiments covered a broad range of wave height conditions and steepness ε as shown in Table 2. Here, T_p is the peak wave period, ε is defined as the ratio between the significant wave height H_s and the average wavelength L_m estimated from the average zero-crossing period T_z via the linear dispersion (water depth $d = 16$ m). Experiment 3, with a much higher wind speed, exhibited the largest H_s / L_m ratio among the three imaged wave fields and the acquired videos confirmed the occurrence of widespread breaking.

The stereo reconstruction of the wave surface yields a four dimensional (4-D) manifold $Z=\eta(X,Y;t)$ defined on a three-dimensional (3-D) space-time volume *V* with sides X_{max}=35 m, Y_{max}=35 m and t_{max}~30 min along *X*,*Y* and *t*, respectively. As an example, from Experiment 2 horizontal and vertical projections of the wave surface manifold are shown in Fig. 3. *WASS* estimates are validated against reference point time series measurements of the wave surface elevation provided by instruments available at *Acqua Alta*: wired wave gauges and an AWAC ADCP profiler. The gauge accuracy is ~1 cm and the sampling frequency is at 4 Hz, whereas AWAC is accredited for accuracies of 1 cm and 2° in

wave elevation and direction, respectively, and sampling rate at 2 Hz. The comparisons are performed as follows: we select several virtual point probes within the reconstructed area (Bottom-left of Fig. 3) in order to extract the associated time series of the stereo reconstructed wave surface displacements (Bottom-right of Fig. 3). Given these, various statistical and spectral properties of waves are computed and compared against those obtained from *Acqua Alta* instruments, hereafter labeled as CNR as shown in Table 3. Here, the peak period T_p is relative to the spectral peak of the frequency spectrum. Estimates of the significant wave heights H_{mo} and $H_{1/3}$, and wave periods T_m and T_z follow from a zero-crossing analysis of the extracted time series low-pass filtered at roughly 2.0 Hz. The largest wave surface height estimated during the experiments is denoted as H_{max}. Such comparisons for different wave conditions clearly prove that the accuracy of *WASS* measurements is comparable to that of more traditional wave instruments. In particular, the difference between *WASS* and CNR wave height estimates are of the order of 1-2 cm.

Table 1 - 2009-2010 *WASS* stereo experiments at *Acqua Alta*. Angle *Dir* denotes wind direction, measured clockwise from geographic North.

Exp #	Wind [m/s, *Dir* (° N)]	Starting date and hour	Frame rate [Hz]	Frames #	Duration [s]
1	6.5, 133.0 Sirocco Breeze	2009/06/05 1428 UTC	10	6000	600
2	9.6, 51.2 Bora	2009/10/14 0755 UTC	10	21000	2100
3	17.9, 67.5 Bora	2010/03/09 1120 UTC	5	9000	1800

Table 2 - Wave conditions during the *WASS* experiments at *Acqua Alta*. H_s: Significant wave height, T_p: peak wave period, T_z: zero up-crossing period, L_m: mean wave length and ε: steepness (Estimates from *Acqua Alta* instruments).

Exp #	Date	H_s [m]	T_p [s]	T_z [s]	L_m [m]	ε
1	2009/06/05	0.47	4.34	2.91	13	0.03
2	2009/10/14	1.09	4.59	3.51	19	0.06
3	2010/03/09	2.16	6.37	4.62	33	0.07

Table 3 – Comparison between *WASS* and CNR estimates of wave parameters. The angle *Dir* denotes the mean wave direction measured clockwise from the geographic North (*Dir* depends upon the platform orientation, which is known up to an error ~3°). During Experiment 1, H_{mo}, $H_{1/3}$, and *Dir* were not available.

		H_{m0} [m]	$H_{1/3}$ [m]	H_{max} [m]	T_p [s]	T_z [s]	*Dir* [° N]
Exp 1	CNR	-	0.47	0.68	-	2.91	-
	WASS	0.45	0.42	0.83	4.34	3.09	148.5±3
Exp 2	CNR	1.13	1.09	2.03	4.59	3.51	65.0±3
	WASS	1.15	1.10	2.18	4.83	3.62	59.5±3
Exp 3	CNR	2.23	2.16	3.80	6.37	4.62	69.7±3
	WASS	2.17	2.16	3.95	6.36	4.85	70.1±3

Wave Statistics

From Experiment 3, consider the ensemble of the time series of the stereo reconstructed wave displacements extracted at several virtual probes as those shown in Fig. 3. The time series are filtered above 1.0 Hz to remove the noise floor of the associated frequency spectra, with variations of the wave variance less than 0.5%. The empirical wave height distribution is then estimated and shown in Fig. 4. A fair agreement with the normalized Boccotti asymptotic form (Boccotti, 2000; Tayfun and Fedele, 2007)

$$P(H > h) = \exp\left(-\frac{h^2}{4\sigma^2(1+\psi^*)}\right) \tag{1}$$

is observed. Here, the parameter ψ^* depends upon the first minimum of the wave covariance and σ is the standard deviation of the wave surface. In particular, the average value over the time series ensemble is $\psi^* \approx 0.69$. Note the deviations from Boccotti's model, which may be due in part to wave breaking and to the stochastic dependence of the time series extracted at the virtual probes, which are too close compared to the mean wavelength. Further, the observed crest/trough statistics is compared against the Tayfun-Fedele (TF) and Forristall (F) models. The TF distributions for crest (C) and trough (T) heights are given, respectively, by (Tayfun and Fedele, 2007; Fedele, 2008)

$$P(C > h) = \exp\left(-\frac{Z_c^2}{2}\right)\left(1 + \frac{\Lambda}{64}z^2(z^2 - 4)\right) \tag{2}$$

$$P(T > h) = \exp\left(-\frac{z^2}{2}(1+0.5\mu z)^2\right)\left(1 + \frac{\Lambda}{64}z^2(z^2 - 4)\right) \tag{3}$$

where, Z_c is derived from the quadratic equation $z = Z_c + \mu Z_c^2/2$, with $z = h/\sigma$ and μ as a characteristic parameter that measures wave steepness (Tayfun, 1986; Fedele and Tayfun, 2009) and Λ is a measure of third order nonlinearities due to both bound and free waves that depends upon the fourth order cumulants of the wave surface η (Tayfun and Fedele, 2007). For the data set at hand $\Lambda \cong 0$ and second order nonlinearities are dominant. The wave steepness can be estimated directly from data via time averages as $\mu = <\eta^3>$, where $<\bullet>$ denotes expectation. However, these estimators are usually statistically unstable. A stable estimate for μ can be defined from the moments of the wave spectrum as (Fedele and Tayfun, 2009)

$$\mu_a = \mu_m(1 - \nu + \nu^2) \tag{4}$$

where ν is the spectral bandwidth given by

$$\nu = \sqrt{m_0 m_2/m_1^2 - 1} \tag{5}$$

where $m_j = \int \omega^j S(\omega)d\omega$ are the spectral moments, and μ_m is the steepness for narrowband waves, i.e. as $\nu \to 0$, that is (Tayfun, 1986)

$$\mu_m = \sigma \omega_m^2/g \tag{6}$$

with $\omega_m = m_1/m_0$ as the mean up-crossing frequency. For Experiment 3, the observed values for these parameters are given by $\mu = 0.080$, $\mu_m = 0.090$, $\mu_a = 0.068$ and $\nu = 0.52$. For comparison, we consider the Forristall model (Forristall, 2000) for crest heigths given by

$$P(C > z) = \exp\left[-\left(\frac{z}{4\alpha}\right)^\beta\right]. \tag{7}$$

The pair of coefficients (α, β) depends upon the steepness parameter $S_1 \approx 0.071$ and the Ursell number $U_r \approx 0$. Drawing from Forristall (2000), for unidirectional (2-D) and multidirectional (3-D) seas ($\alpha_2 = 0.374$, $\beta_2 = 1.848$) and ($\alpha_3 = 0.372$, $\beta_3 = 1.874$), and the associated models from (7) are referred to as F2 and F3, respectively. The observed crest and trough exceedance probabilities are given in Fig. 5. Good is the

agreement with both the TF and F. The observed trough statistics fairly agrees with the TF model as well.
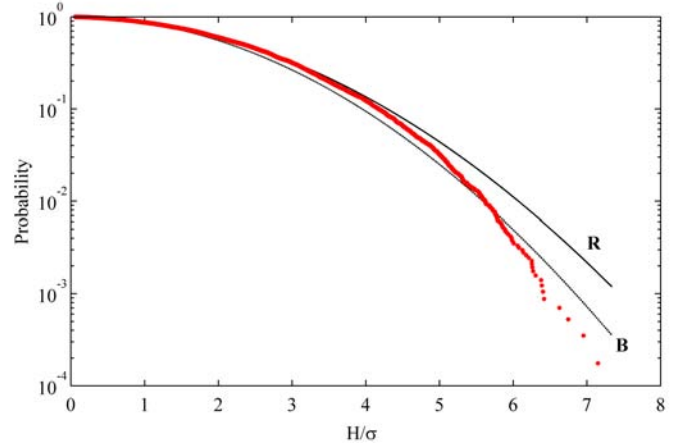

Fig. 4 - Experiment 3. Wave height exceedance probability. Rayleigh (R) and Boccotti (B) theoretical distribution are superimposed.
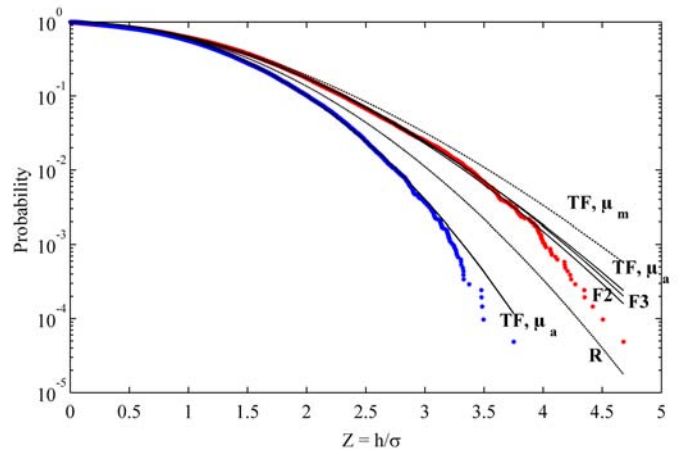

Fig. 5 - Experiment 3. Empirical wave crest (red dots) and trough (blue dots) exceedance probabilities against theoretical distributions: R: Rayleigh; TF: Tayfun-Fedele model with steepness μ; F2: 2-D Forristall; F3: 3-D Forristall.
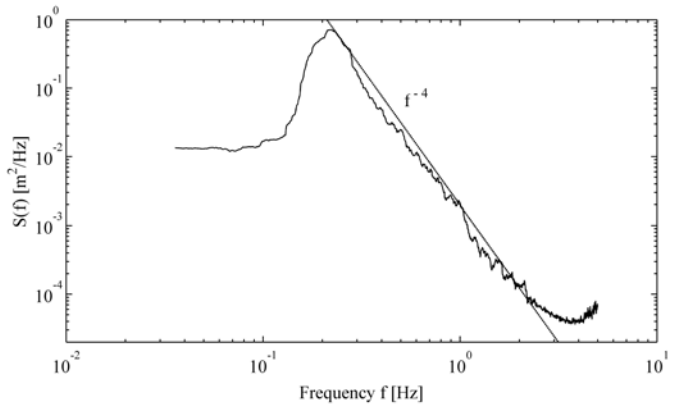

Fig. 6 - Experiment 2. Observed mean frequency spectrum $S(f)$ estimated from time series extracted at 40 virtual probes within the imaged area (Fig. 3). Nyquist frequency = 5.0 Hz.

Wave Spectra

From Experiment 2, consider the ensemble of the surface displacements time series extracted at 40 virtual probes in the *XY* plane of Fig. 3. The mean frequency spectrum $S(f)$ is estimated by averaging over the actual spectra of the ensemble and shown in Fig. 6. An inertial range that decays as f^{-4} is observed in agreement with Zakharov's theory (Zakharov, 1999). However, a noise floor is noticed approximately above 2.5 Hz and the f^{-5} Phillips' regime is not observed (Phillips, 1977; Newell and Zakharov 2008).

The mean directional spectrum $S(k_X,k_Y)$ is obtained by averaging the 2-D Fourier Transforms of the reconstructed sea surface snapshots from Experiment 2. Fig. 7 (Left panel) shows the omnidirectional spectrum $S(k)$ that proceeds by numerically integrating $S(k_X,k_Y)$ over all the directions. In agreement with results of Zakharov (1999) and experiments of Hwang et al. (2000), the omnidirectional wavenumber spectrum $S(k)$ tail decays roughly as $k^{-2.5}$. The associated saturation spectrum (Right panel of Fig. 7) shows that the tail decays with power higher than 2.5 for wavenumbers above 3 rad/m, and some noise appears approximately above 10 rad/m, which clouds the Phillips' regime due to breaking.
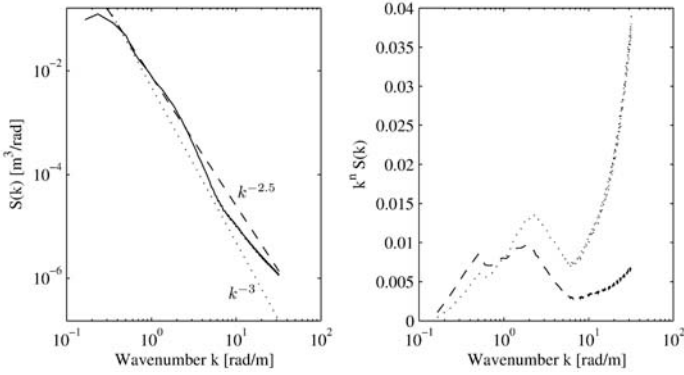

Fig. 7 - Experiment 2: (Left) omnidirectional wavenumber spectrum S(*k*) and (right) associated saturation spectra $k^n S(k)$, with *n*=3 (dot line) and *n*=2.5 (dash line).
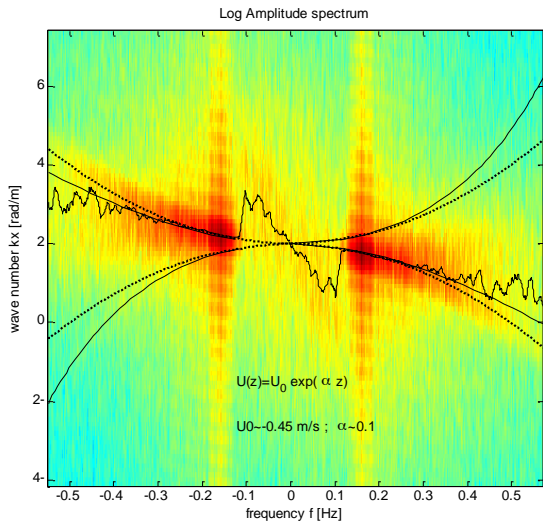

Fig. 8 - Experiment 3: wavenumber-frequency spectrum (log scale), observed dispersion curve (black line), theoretical dispersion curve without current (dot line) and with current (solid line).
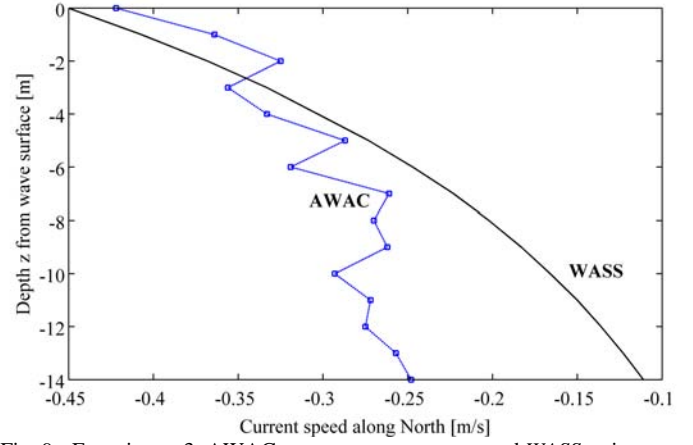

Fig. 9 - Experiment 3: AWAC current measurements and *WASS* estimates.

The 3-D wavenumber-frequency spectrum $S(k_X,k_Y;\omega =2\pi f)$ can be estimated by Fourier transforming the entire three-dimensional $z = \eta(x,y,t)$ wave surface data both in space and in time. The regions of non-zero amplitude identify the wave dispersion curve, from which the vertical profile of the current flow velocity underneath the wave surface can be estimated as follows. From the AWAC measurements available during Experiment 3, the underwater current is directed mostly along the North direction *s*, and it varies with depth as shown in Fig. 9. In order to estimate the current speed profile from *WASS* data, we extract a slice of the 3-D spectrum along the direction *s* as shown in Fig. 8. The estimated *k-ω* spectrum smears out around the observed dispersion relation curve because of the well-known spectral leakage due to the finite extension of the data sets (see, for example, Krogstad and Trulsen, 2010). Below the spectral peak, the observed dispersion curve deviates from the theoretical linear counterpart with no current (black line), viz.

$$k = \pm \frac{(2\pi f)^2}{g} \tag{8}$$

in agreement with Krogstad and Trulsen (2010), who observed similar deviations in simulated spectra of the Dysthe equations, as an unexpected effect of the spectral leakage. Above the spectral peak, the Doppler-shift causes the observed wave dispersion to deviate from its linear counterpart (8). Such deviations can be related to the unknown current speed profile $U(z)$ using the modified dispersion relation (see, for example, Phillips, 1977; Boccotti, 2000)

$$k = \pm \frac{(2\pi f - U_0 k)^2}{g} \tag{9}$$

which accounts for a uniform current U_0 collinear with the direction of wave propagation. Here, U_0 is an average speed that accounts for the effects of long-wave modulation on short waves and the variability of current with depth (Stewart and Joy, 1974). Further, U_0 is a function of k via $U(z)$ since longer waves are affected by current flows near the sea bottom, whereas shorter waves are affected by currents near the surface, viz. (Steward and Joy, 1974)

$$U_0(k) = 2k \int_{-\infty}^{0} U(z) \exp(2kz)\, dz \tag{10}$$

Estimating the profile $U(z)$ from Eqs. (9) and (10) is an ill-posed inverse problem that requires regularization. To do so, we add the constraint of an exponential profile and express U as

$$U(z) = U_{max} \exp(\alpha z), \quad z \le 0, \tag{11}$$

and from (9) it follows that

$$U_0(k) = \frac{2kU_{max}}{2k+\alpha}. \tag{12}$$

Here, the wavenumber k is a function of the frequency $f=\omega/2\pi$ via the theoretical dispersion relation (8). The best values for U_{max} and α that match the observed dispersion curve (Fig. 8) with the theoretical form (9) are estimated as $U_{max}=-0.45$ m/s and $\alpha = 0.1$ m^{-1} respectively. The *WASS* estimate of the current profile follows from Eq. (11) and it is shown in Fig. 9 in comparison to that measured by the AWAC instrument operational at *Acqua Alta*.
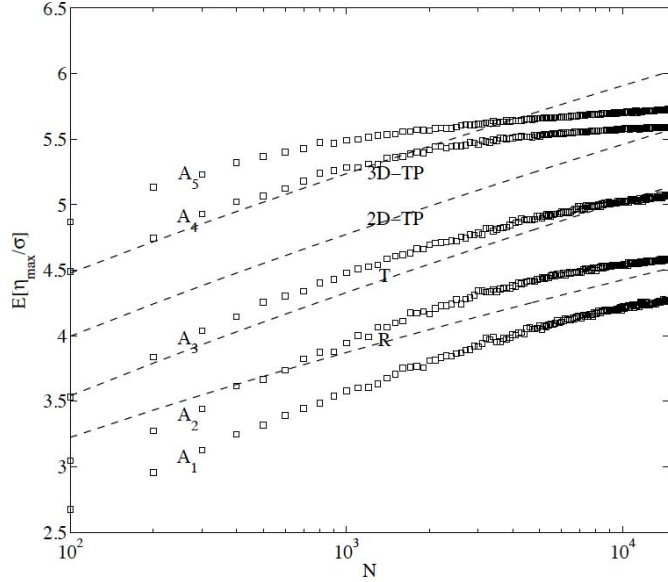

Fig. 10 - Experiment 2: Expected maximum of the surface height η_{max}/σ over the area A as function of the number N of snapshots against theoretical models $A_1=3\times10^{-3}$, $A_2=1$, $A_3=10$, $A_4=100$, and $A_5=534$ m^2. R: Rayleigh, T: Tayfun, TP Tayfun-Piterbarg.
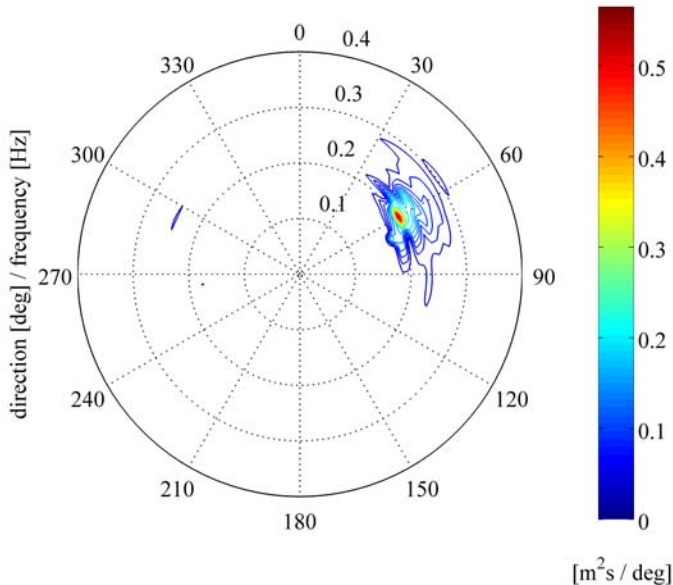

Fig. 11 – Experiment 2: directional spectrum estimated using EMEP method. Wave direction is measured clockwise from the geographic North. Resolution is 2° and 10^{-2} Hz.
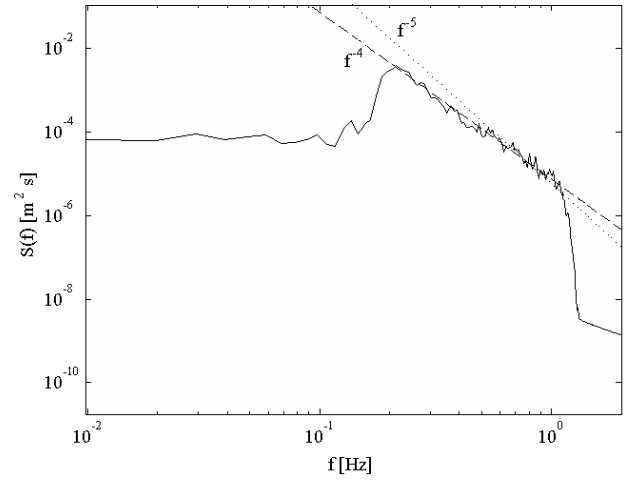

Fig. 12 – Experiment 2: omnidirectional frequency spectrum $S(f)$.

Table 4 – Experiment 2: comparison of synthetic parameters of the sea state. CNR: point probe operating at *Acqua Alta*; *WASS*: Wave Acquisition Stereo System; EMEP: Directional analysis using Extended Maximum Entropy Principle. The angle *Dir* denotes the mean wave direction measured clockwise from the geographic North.

	CNR	*WASS*	EMEP
H_{m0} [m]	1.13	1.15	1.11
T_p [s]	4.59	4.83	4.88
Dir [°N]	65.00	59.50	60.00

SPACE-TIME EXTREME VALUE ANALYSIS

In the following we will investigate the extreme value statistics of the largest amplitude of the wave surface η over a given area A. To do so, consider the sequence $\{\xi_1, \xi_2, ..., \xi_N\}$ of the instantaneous normalized maximum $\xi(t) = \eta_{max}(t)/\sigma$ of η observed over a region of the field of view of area A. As a reference statistics consider that of the expected maximum crest height $C_\beta(N)$ of N waves whose parent statistical distribution follows the general law

$$P(h > z) = z_1^\beta \exp(-z_1^2/2), \quad \beta \geq 1 \tag{13}$$

where the linear amplitude z_1 satisfies the Tayfun quadratic equation $z = z_1 + \mu z_1^2/2$ (Tayfun, 1986) to account for second order nonlinearities. In this case, the expected maximum crest height depends upon the parameter β and it is given, according to Gumbel (1958), by

$$C_\beta(N) = h_N + \frac{\mu}{2}h_N^2 + \gamma_e \frac{1+\mu h_N}{h_N - \beta/h_N}, \tag{14}$$

where h_N satisfies $h_N^\beta \exp(-h_N^2/2) = 1/N$. For $\beta = 0$ the Tayfun model is recovered, as it should be. The 2-D and 3-D Tayfun-Piterbarg models are obtained for β equal to 1 and 2, respectively. The expected maximum $\xi_{max}(N)$ is computed according to the Gumbel statistics $C_\beta(N)$ of Eq. (14) and compared it against the observed expected maximum wave elevation in Fig. 10 (data from Experiment 2). As the area increases, the observations deviate from the 1D Tayfun model staying between the 2D and 3D Tayfun-Piterbarg statistics. Note that the surface maximum estimates over the smallest area ($A=3\times10^{-3}$ m^2)

are practically those observed at a given point, and hereafter referred to as $\xi_{max,p}$. Indeed, in this case the mean wavelength L_m is much larger than the length $A^{1/2}$ of the area's side. Clearly, as the area's size increases, so does the expected areal maximum ξ_{max}. For example, over the area $A \sim 534$ m^2 $\xi_{max} \approx 1.34\xi_{max,p}$. More rigorous stochastic models can be applied to describe space-time extremes and their expected values (Piterbarg, 1995; Adler and Taylor, 2007). Indeed, the wave surface can be modeled as a three-dimensional homogeneous Gaussian random field $\eta(x,y,t)$ over a space-time volume Ω of dimensions X, Y and D respectively. According to Fedele (2012), in a Gaussian sea state of duration D the expected maximum wave surface height $\xi_{max} = \bar{\eta}_{max}/H_s$ over the area $A=XY$ is given, according to Gumbel (1958), by

$$\xi_{max} = \zeta_0 + \frac{\gamma_e}{16\zeta_0 - \frac{F'(\zeta_0)}{F(\zeta_0)}} \quad (15)$$

where $\gamma_e = 0.5772$, the prime denotes derivative and ζ_0 satisfies

$$F(\zeta)\exp(-8\zeta^2) = 1 \quad (16)$$

with

$$F(\zeta) = 16M_3\zeta^2 + 4M_2\zeta + M_1 \quad (17)$$

Here, M_3, M_2, M_1 are the average number of 3-D, 2-D and 1-D waves that can occur in the space-time volume of X, Y, D dimensions and they all depend upon the directional wave spectrum $S(f,\theta)$ (see appendix). The expected maximum crest height $\xi_{max,p}$ at a given point follows from Eq. (15) by setting $M_3=M_2=0$.

Note that Eq. (15) relies on the assumption of stochastic independence of large waves, which holds for weakly non-Gaussian fields dominated by second order nonlinearities, or short-crested seas considered in this work. Clearly, in narrow-banded seas the areal effects are negligible and Eq. (15) reduces to the time point estimates. However, in this case the wave surface is affected by nonlinear quasi-resonant interactions and fourth-order cumulants increase beyond the Gaussian threshold (see, for example, Fedele et al. 2011). To account for such deviations, a naïve approach would be to simply replace in (14) the Rayleigh/Tayfun distribution with Gram-Charlier (GC) type models, such as those developed by Tayfun and Fedele (2007) or Fedele (2008). Indeed, GC models have been shown to describe the effects of modulation instability on the wave statistics (see, for example, Fedele et al., 2011). However, in such narrow-band sea states individual waves are correlated (see for example, Janssen, 2003) and Eq. (15), even with a GC model, loses its validity and yields conservative estimates as an upper bound. So does the extreme value analysis proposed by Janssen (2006), which follows the classical approach by Gumbel (1958) based on wave independency. Thus, it is necessary to develop a stochastic model that can smoothly bridge narrow-band and short-crested conditions. Such model would require taking into account the correlation between neighboring waves and it should depend upon the joint probability distribution of successive extremes (see, for example, Fedele, 2005). Such studies are in progress and will be discussed elsewhere.

In the following, in order to apply Eq. (15) we proceed with estimating the directional spectrum using a modified version of the MATLAB® DIWASP v1.3 toolbox (Johnson, 2004) for the Extended Maximum Entropy Principle (EMEP, Hashimoto et al, 1994). For Experiment 2, the polar representation of the estimated $S(f,\theta)$ is reported in Fig. 11. Wave parameters calculated from the EMEP spectrum are in good agreement with those measured by WASS and CNR instruments (see Table 4). The associated omnidirectional frequency spectrum is shown in Fig. 12.

Given $S(f,\theta)$, from Eq. (15) we can estimate the ratio between the expected surface maximum ξ_{max} and that at a point, viz. $\xi_{max,p}$, as function of the area A. For example, Fig. 13 reports such predictions based on Eq. (15), which are the theoretical average over an ensemble of realizations of a sea state with the estimated spectrum $S(f,\theta)$. In the same Figure, we report the same ratio observed from WASS measurements of the surface height (just one realization), which fairly agree with the theoretical estimates based on Eq. (15). In particular, for $A=534$ m^2 the ratio $r = \xi_{max}/\xi_{max,p} \sim 1.36$ in agreement with the predictions of Fig. 10.
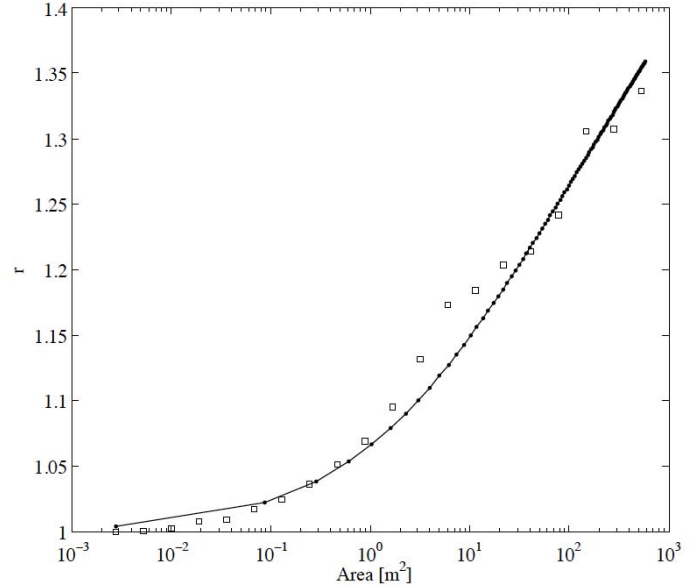

Fig. 13 – Experiment 2: (solid line) theoretical predictions of the ratio $r = \xi_{max}/\xi_{max,p}$ between the expected maximum surface height ξ_{max} over an area and that expected at a point, viz. $\xi_{max,p}$ and (squares) observed WASS ratios from the measured sea state.

CONCLUSIONS

We have deployed a Wave Acquisition Stereo System (WASS) at the oceanographic platform Acqua Alta off the Venice coast in Italy. As a video observational technology, WASS is able to provide a multi-dimensional image of the oceanic state around the tower under both Bora and Sirocco Breeze wind conditions. Advanced stereo techniques based on the epipolar geometry are exploited to obtain 3-D reconstructions of the sea surface both in space and in time. The accuracy of WASS measurements is proven to be comparable to that of more traditional wave instruments. Further, the directional spectrum is estimated directly by averaging over the reconstructed spatial snapshots. The statistics of crest and trough heights, as well as that of crest-to-trough heights estimated via WASS agree very well with known theoretical models, such as the Forristall and Tayfun-Fedele distributions for crests and the Boccotti model for wave heights.

We also proposed novel techniques for estimating wave spectra, dispersion and currents from the stereo-reconstructed wave surface. Finally, a statistical analysis of the reconstructed spatial snapshots based on Adler/Piterbarg stochastic theories reveals that the expected maximum wave surface height over an area is larger than that expected at a given point in space.

APPENDIX

The coefficients in Eq. (17) are given by

$$M_3 = 2\pi \frac{D}{T} \frac{X}{L_x} \frac{Y}{L_y} \alpha_{xyt}$$

$$M_2 = \sqrt{2\pi} \left(\frac{DX}{T L_x} \sqrt{1-\alpha_{xt}^2} + \frac{DY}{T L_y} \sqrt{1-\alpha_{yt}^2} + \frac{XY}{L_x L_y} \sqrt{1-\alpha_{xy}^2} \right),$$

$$M_1 = \frac{D}{T} + \frac{X}{L_x} + \frac{Y}{L_y}.$$

which depend upon mean wave period $\overline{T}$, mean wavelengths in X and Y directions, $\overline{L_x}$ and $\overline{L_y}$, viz.

$$\overline{T} = 2\pi \sqrt{\frac{m_{000}}{m_{002}}}, \qquad \overline{L_x} = 2\pi \sqrt{\frac{m_{000}}{m_{200}}}, \qquad \overline{L_y} = 2\pi \sqrt{\frac{m_{000}}{m_{020}}}$$

and

$$\alpha_{xt} = \frac{m_{101}}{\sqrt{m_{200} m_{002}}}, \quad \alpha_{yt} = \frac{m_{011}}{\sqrt{m_{020} m_{002}}}, \quad \alpha_{xy} = \frac{m_{101}}{\sqrt{m_{200} m_{020}}}.$$

$$\alpha_{xyt} = \sqrt{1-\alpha_{xt}^2 - \alpha_{yt}^2 - \alpha_{xy}^2 + 2\alpha_{xt}\alpha_{yt}\alpha_{xy}}.$$

Here, m_{ijk} are the moments of the directional spectrum $S(f,\theta)$ given by

$$m_{ijk} = \iint k_x^i k_y^j f^k S(f,\vartheta) df d\vartheta .$$

REFERENCES

Adler, RJ (1981). *The Geometry of Random Fields*, John Wiley, 275 pp.

Adler, RJ (2000). "On excursion sets, tube formulae, and maxima of random fields", *Annals of Applied Probability*, Vol 10, pp 1-74.

Adler, RJ, and Taylor, JE (2007). *Random fields and geometry*, Springer Monographs in Mathematics, Springer, 454 pp.

Banner, ML, Jones, SF, Trinder, JC (1989). "Wavenumber spectra of short gravity waves", *J Fluid Mech*, Vol 198, pp 321-344.

Baxevani, A, and Richlik, I (2004). "Maxima for Gaussian seas". *Ocean*

Benetazzo, A (2006). "Measurements of short water waves using stereo matched image sequences", *Coastal Engineering*, Vol 53, pp 1013-1032.

Benetazzo, A, Fedele, F, Gallego, G, Shih, PC, Yezzi, A (2012). "Offshore stereo measurements of gravity waves", *Coastal Engineering*, in press, doi: 10.1016/j.coastaleng.2012.01.007.

Boccotti, P (2000). *Wave mechanics for ocean engineering*, Elsevier Science, 496 pp.

Fedele, F (2005). "Successive wave crests in Gaussian seas", *Probabilistic Engineering Mechanics*, Vol 20(4), pp 355-363.

Fedele, F (2008). "Rogue Waves in Oceanic Turbulence", *Physica D*, Vol 237(14-17), pp 2127-2131.

Fedele, F, and Tayfun, MA (2009). "On nonlinear wave groups and crest statistics", *J Fluid Mech*, Vol 620, pp 221-239.

Fedele F, Benetazzo, A, and Forristall, GZ (2011). "Space-time waves and spectra in the Northern Adriatic Sea via a Wave Acquisition Stereo System". *30th ASME Int. Conf. Offshore Mechanics and Arctic Eng*, Rotterdam, The Netherlands, paper OMAE2011-49924.

Fedele, F (2012). "Space-time extremes of sea storms", *J Phys Oceanogr,* under review.

Forristall, GZ (2000). "Wave crests distributions: observations and second order theory", *J Phys Oceanogr*, Vol 38(8), pp 1931–1943.

Forristall, GZ (2006). "Maximum wave heights over an area and the air gap problem", in *Proceedings of the ASME 2006 25th International Conference on Ocean, Offshore and Arctic Engineering* (OMAE 2006) in Hamburg, Germany.

Forristall, GZ (2007). "Wave crest heights and deck damage in Hurricanes Ivan, Katrina and Rita", in *Proceedings of the Offshore Technology Conference Proceedings* in Houston, USA.

Gallego G, Yezzi, A, Fedele F and Benetazzo, A (2012). "A Variational Stereo Algorithm for the 3-D reconstruction of ocean waves". *IEEE Transations on Geoscience and Remote Sensing*, Vol 49(11), pp 4445-4457.

Goda, Y (1999). *Random seas and Design of Maritime Structures*, World Scientific, 443 pp.

Gumbel, E. J., 1958: *Statistics of Extremes*. New York: Columbia University Press, 1-373.

Hashimoto, N, Nagai, T, Asai, T (1994). "Extension of the Maximum Entropy Principle Method for Directional Wave Spectrum Estimation", *Proc 24th Int. Conf. Coastal Engineering (Kobe, ACSCE),* pp 232-246.

Holthuijsen, LH (1983). "Observations of the directional distribution of ocean wave energy", *J Phys Oceanogr*, Vol 13, pp 816-827.

Hwang, P, Wang, D, Walsh, E, Krabill, W, Swift, R (2000). "Airborne measurements of the wavenumber spectra of ocean surface waves, part I: spectral slope and dimensionless spectral coefficient", *J Phys Oceanogr*, Vol 30, pp 2753–2767.

Jahne, B (1993). *Spatio-Temporal Image Processing - Theory and Scientific Applications*, Springer-Verlag, 208 pp.

Janssen, P.A.E.M., 2003: Nonlinear Four-Wave Interactions and Freak Waves. *J. Phys. Oceanogr.*, **33**, 863-884.

Johnson, D (2004). "DIWASP, a directional wave spectra toolbox for MATLAB®: User Manual". *Research Report WP-1601-DJ (V1.1)*, Centre for Water Research, University of Western Australia.

Krogstad, HE. Trulsen, K (2010). "Interpretations and observations of ocean wave spectra", Ocean Dynamics, Vol 60 (4), pp 973–991.

Ma, Y, Soatto, S, Kosecka, J, Shankar Sastry, S (2004). *An invitation to 3-D vision: from images to geometric models*, Springer-Verlag, 526 pp.

Mori N. and PAEM Janssen, 2006: On kurtosis and occurrence probability of freak waves. *J. Phys. Oceanogr.*, **36(7)**, 1471-1483.

Newell, AC, Zakharov, VE (2008). "The role of the generalized Phillips' spectrum in wave turbulence", *Phys Lett A,* Vol 372 (23), pp 4230-4233.

Phillips, OM (1977). *The dynamics of the upper ocean*, Cambridge University Press, 344 pp.

Piterbarg, V (1995). *Asymptotic Methods in the Theory of Gaussian Processes*, AMS ser. Translations of Mathematical Monographs, Vol 148, 205 pp.

Shemdin, OH, Tran, HM, Wu, SC (1988). "Directional Mesurements of short ocean waves with stereography", *J Geophys Res,* Vol 93, pp 13891-13901.

Tayfun, MA (1979). "Joint Occurrences in Coastal Flooding", *J Waterway, Port, Coast and Ocean Eng*, ASCE, Vol 105(WW2), pp 107-123.

Tayfun, MA (1986). "On narrow-band representation of ocean waves. Part I: Theory", *J Geophys Res*, Vol 1(C6), pp 7743-7752.

Tayfun, MA, and Fedele, F (2007). "Wave-height distributions and nonlinear effects", *Ocean Engineering*, Vol 34(11-12), pp 1631-1649.

Zakharov, VE (1999). "Statistical theory of gravity and capillary waves on the surface of a finite-depth fluid", *Eur J Mech B Fluids*, Vol 18(3), pp 327-344.